



Molecular simulations of C₆₀ self-assembly on metal-adsorbed Si(111) surfaces

Oleg A. Utas, Dmitry A. Olyanich, Vsevolod V. Mararov, Tatiana V. Utas, Andrey V. Zotov, and Alexander A. Saranin

Citation: *Journal of Vacuum Science & Technology B* **34**, 051806 (2016); doi: 10.1116/1.4961906

View online: <http://dx.doi.org/10.1116/1.4961906>

View Table of Contents: <http://scitation.aip.org/content/avs/journal/jvstb/34/5?ver=pdfcov>

Published by the AVS: Science & Technology of Materials, Interfaces, and Processing

Articles you may be interested in

Modeling charge transport in C₆₀-based self-assembled monolayers for applications in field-effect transistors
J. Chem. Phys. **140**, 204702 (2014); 10.1063/1.4876035

Molecular orientation and lattice ordering of C₆₀ molecules on the polar FeO/Pt(111) surface
J. Chem. Phys. **136**, 024701 (2012); 10.1063/1.3676087

Self-assembly of C₆₀ monolayer on epitaxially grown, nanostructured graphene on Ru(0001) surface
Appl. Phys. Lett. **100**, 013304 (2012); 10.1063/1.3673830

Molecular orientations and interfacial structure of C₆₀ on Pt(111)
J. Chem. Phys. **134**, 044707 (2011); 10.1063/1.3530289

Polarized near-edge x-ray-absorption fine structure spectroscopy of C₆₀-functionalized 11-amino-1-undecane thiol self-assembled monolayer: Molecular orientation and Evidence for C₆₀ aggregation
J. Chem. Phys. **122**, 154703 (2005); 10.1063/1.1880952

A promotional banner for the AVS 63rd International Symposium & Exhibition. The banner features a background image of a keyboard and a guitar. On the left, the AVS logo is displayed with the website address www.avs.org below it. The main text in the center reads 'AVS 63RD International Symposium & Exhibition' in a large, orange, serif font. Below this, 'MUSIC CITY CENTER' is written in a smaller, white, sans-serif font. At the bottom, the dates 'Symposium: November 6-11, 2016 | Exhibit: November 8-10, 2016' are listed in a white, sans-serif font. On the right side, there is a graphic of a guitar and a sign that says 'ERB MUSIC'.

Molecular simulations of C₆₀ self-assembly on metal-adsorbed Si(111) surfaces

Oleg A. Utas, Dmitry A. Olyanich, Vsevolod V. Mararov, and Tatiana V. Utas
Institute of Automation and Control Processes FEB RAS, 5 Radio Street, 690041 Vladivostok, Russia
and School of Natural Sciences, Far Eastern Federal University, 690950 Vladivostok, Russia

Andrey V. Zotov^{a)}

Institute of Automation and Control Processes FEB RAS, 5 Radio Street, 690041 Vladivostok, Russia; School of Natural Sciences, Far Eastern Federal University, 690950 Vladivostok, Russia; and Department of Electronics, Vladivostok State University of Economics and Service, 690600 Vladivostok, Russia

Alexander A. Saranin

Institute of Automation and Control Processes FEB RAS, 5 Radio Street, 690041 Vladivostok, Russia
and School of Natural Sciences, Far Eastern Federal University, 690950 Vladivostok, Russia

(Received 4 June 2016; accepted 17 August 2016; published 29 August 2016)

The authors have proposed a simulation procedure for the evaluation of energetics of C₆₀ islands on crystalline surfaces that allows questions relating to shape, size, and orientation of the islands to be addressed. Simulation consists of placing a patch of close-packed C₆₀ array of a given shape and size on a surface potential relief and finding energy minima by variation of island position and orientation. Upon appropriate adjustment of the surface potential relief, simulations reproduce well all the main results of the scanning tunneling microscopy observations. For C₆₀ islands forming on In-adsorbed Si(111) $\sqrt{3} \times \sqrt{3}$ -Au and pristine Si(111) $\sqrt{3} \times \sqrt{3}$ -Ag surfaces, the optimal surface relief shows up as a periodic array of cosine-shaped peaks. The proposed approach provides a hint for understanding the driving mechanisms of C₆₀ self-assembly, and, in principle, it can be applied to other adsorbate-substrate systems. © 2016 American Vacuum Society.

[<http://dx.doi.org/10.1116/1.4961906>]

I. INTRODUCTION

Since the discovery of the C₆₀ buckminsterfullerene in 1985,¹ fullerenes, carbon molecules with a cage structure, have attracted widespread attention due to their unique properties and prospects for device applications. In particular, self-assembled growth of fullerene monolayers on various substrates is an actively developed research area. Numerous experimental investigations have been conducted in this field utilizing a variety of surface-sensitive techniques, including scanning tunneling microscopy and spectroscopy (STM),^{2–14} x-ray diffraction,^{15–18} low-energy electron diffraction,^{10,19–23} photoemission spectroscopy,^{6,15,24} etc. However, the most advanced and reliable results have been obtained only when the experimental observations were combined with theoretical considerations (e.g., as has been done in all the works referred to above). Among other theoretical approaches, density functional theory (DFT) calculations occupy the most prominent place.^{2–10,15–31} They demonstrate a great efficiency in resolving many complicated subjects related to fullerene interactions with surfaces, such as C₆₀ adsorption geometry, including the cases of substrate reordering (e.g., nanopit formation), orientation of fullerene on a surface and simulation of corresponding STM images with intramolecular resolution, charge transfer and change of fullerene electronic properties upon adsorption onto a given surface, fullerene manipulations, etc. Note that

all these characteristics refer primarily to individual fullerenes, which is a natural consequence of computational limitations for many-atom systems.

As for fullerene islands, their formation has been treated using nucleation rate theory³² or kinetic Monte Carlo simulations via analysis of island number density,^{11,12} island size distribution,^{11,13} or capture zone distribution¹⁴ as a function of growth parameters, temperature, and deposition rate. This approach enables determination of a critical island size, a surface diffusion barrier, and a binding energy gained in forming the critical island.

However, a number of questions related to fullerene self-assembly cannot really be dealt with using the above theoretical approaches. In particular, we could mention elucidating the origin of occurring orientations of C₆₀ close-packed arrays with respect to crystal substrates or developing C₆₀ island shapes. Thus, novel approaches are required to fill this gap. These might be very sophisticated, like kinetic Monte Carlo simulations used for studying the C₆₀ layer growth on pentacene^{33–36} or graphite,³⁷ but could also be relatively simple, such as that used in the present work where the simulation procedure is based on placing a patch of C₆₀ of a given size, shape, and orientation onto a known or suppositious surface potential relief and evaluating its energy.

In the present work, this approach has been applied to C₆₀ arrays and islands self-assembled on In-adsorbed Si(111) $\sqrt{3} \times \sqrt{3}$ -Au and pristine Si(111) $\sqrt{3} \times \sqrt{3}$ -Ag surfaces. It has been demonstrated that under appropriate adjustment of a shape of a surface potential relief, the simulations reproduce

^{a)}Electronic mail: zotov@iacp.dvo.ru

well the main results of STM observations, including the occurrence of selected orientations of C₆₀ arrays and island shapes, including the development of C₆₀ magic-size islands.

II. SIMULATION AND EXPERIMENTAL DETAILS

Simulations were done in the framework of assumptions as follows:

- (1) A substrate surface is represented by a periodic potential relief which remains unchanged upon fullerene adsorption.
- (2) Fullerenes tend to occupy the lowest-energy sites.
- (3) C₆₀ islands show up essentially as patches of the fullerite monolayer (hexagonal close-packed C₆₀ array) on a substrate surface.

A detailed description of the algorithm used in the simulations is given in the supplementary material.³⁸

Note that the C₆₀-C₆₀ distance in the simulations was fixed for all fullerenes at 10.02 Å, the value of the fullerite layer. In principle, the intermolecular interaction can be taken into account using the corresponding term based on C₆₀-C₆₀ paired potential (e.g., like that calculated in Ref. 39). However, our test simulations for selected C₆₀ islands show that C₆₀-C₆₀ distances vary within the island by less than 0.5%. Note that this is consistent with the results of STM observations of C₆₀ arrays on the In-adsorbed Si(111)√3 × √3-Au (Ref. 40) or pristine Si(111)√3 × √3-Ag (Refs. 41 and 42) surfaces, which demonstrates that C₆₀ self-arrange on these surfaces into close-packed fullerite-layer-like arrays irrespective of the array size, shape, and orientation. Thus, the assumption of the constant C₆₀-C₆₀ distance is proved to be an adequate guess, with the additional merit that it facilitates the calculations.

To check the validity of the simulations, their results were compared with the data acquired in STM studies of C₆₀ growth on In-adsorbed Si(111)√3 × √3-Au and pristine Si(111)√3 × √3-Ag surfaces. A detailed description of the experiments is given elsewhere.^{39,40,43} In brief, experiments were performed with an Omicron VT-STM operating in an ultrahigh vacuum (~2.0 × 10⁻¹⁰ Torr). Atomically clean Si(111)7 × 7 surfaces were prepared *in situ* by flashing to 1280 °C after the samples were first outgassed at 600 °C for several hours. Gold and silver were deposited from Au- and Ag-wrapped tungsten filaments, respectively, indium from a Ta crucible and C₆₀ fullerenes from a Ta boat or Mo crucible. For STM observations, electrochemically etched tungsten tips cleaned by *in situ* heating were employed. All STM images were acquired at room temperature.

III. RESULTS AND DISCUSSION

Let us start with C₆₀ self-assembly on In-adsorbed Si(111)√3 × √3-Au surface and summarize the main available data concerning this system. A pristine Au/Si(111)√3 × √3 surface is typically prepared by depositing about 1 ML Au onto an Si(111)7 × 7 surface held at ~600 °C. Its ideal atomic structure is described by the conjugate honeycomb-chained-trimer (CHCT) model.⁴⁴⁻⁴⁶ The characteristic feature of the real √3 × √3-Au surface is a disordered

meandering domain-wall network.⁴⁷ The domain walls can be melted at temperatures higher than 600 °C, but they restore back upon cooling the sample to room temperature.⁴⁴ However, a stable highly ordered domain-wall-free √3 × √3-Au surface can be formed by adding to it ~0.15 ML of a suitable adsorbate, in particular, In.⁴⁸⁻⁵⁰ In this case, the CHCT arrangement of the original √3 × √3-Au surface is preserved while In forms a two-dimensional adatom gas on the surface. Adatoms are highly mobile at room temperature but they can be frozen in fixed positions upon cooling to ~100 K.

When C₆₀ fullerenes are deposited onto an In-adsorbed Si(111)√3 × √3-Au surface, two types of C₆₀ arrays with different orientations are formed.⁴⁰ In the arrays of the first type (19.1°-rotated arrays), the molecular rows make an angle of ±19.1° with the principal crystallographic directions of the Si(111) surface, i.e., ⟨10 $\bar{1}$ ⟩. In these arrays, all fullerenes exhibit the same STM contrast which can be treated as a sign of a similar bonding state. In the arrays of the second type (0°-rotated arrays), the rows are aligned along the ⟨10 $\bar{1}$ ⟩ directions. A peculiar feature of the 0°-rotated arrays is the characteristic moiré pattern which shows up as a 2D √19 × √19 lattice of fullerenes that look in STM images brighter than other ones. It was recognized that “bright” fullerenes reside directly atop Au trimers of underlying Si(111)√3 × √3-Au surface⁴⁰ and this adsorption site is the most energetically unfavorable one.³⁹

The occurrence of the moiré pattern has been found to affect the growth of 0°-rotated C₆₀ islands, whose shape and size are dictated by minimization of the number of “bright” fullerenes within an island.³⁹ Among the small islands, the most stable are those where the absence of “bright” fullerenes is achieved by adopting unusual noncompact island shapes (e.g., “stadium,” “boomerang,” and “zigzag”) [Fig. 1(a)]. The islands of the larger sizes have the shape of the overlapping hexagons with “bright” fullerenes in their centers. Large 19.1°-rotated C₆₀ islands are also observed [Fig. 1(b)].

The first step for starting simulations is generating appropriate surface potential relief associated with the fullerene interaction with a given surface. An initial hint can be provided by the DFT calculations which yield adsorption energies in selected sites within the surface unit cell. As an example, such a data set for Si(111)√3 × √3-Au surface reconstruction with 1/6 ML In taken from Ref. 39 is shown in Fig. 2. In the cited calculations,³⁹ the DFT-based Vienna *ab initio* simulation package with the projector-augmented wave pseudopotentials and nonlocal van der Waals exchange-correlation function were used to obtain accurate C₆₀-surface adsorption energies. In Fig. 2, one can see that the most stable C₆₀ adsorption site is that in the center of the Si trimer, while the most energetically unfavorable is that in the center of the Au trimer. As a first guess, the potential relief is built using interpolation through available reference points [Fig. 3(a)]. Then, the C₆₀ island (which is essentially a patch, or partial monolayer, of close-packed fulleritelike monolayer) of a given shape and size is superposed on the potential relief. The energy of the island is defined as the sum of energies of all fullerenes divided by the

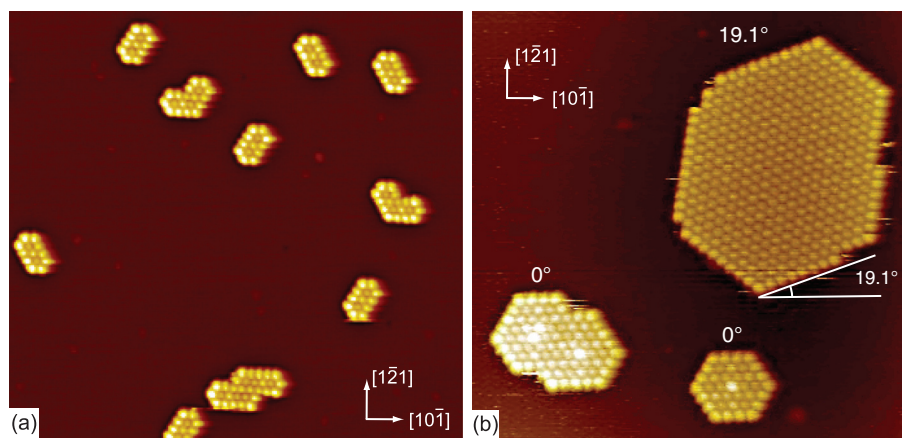


FIG. 1. (Color online) STM images of $45 \times 45 \text{ \AA}^2$ showing the typical C₆₀ islands forming on In-adsorbed Si(111) $\sqrt{3} \times \sqrt{3}$ -Au surface (a) at the early and (b) more late growth stage. Rotational orientations of the islands are indicated with respect to the principal crystallographic directions of the Si(111) surface, $\langle 10\bar{1} \rangle$.

C₆₀ number, where the energy of each fullerene is given by the value of potential in its adsorption site. First, the rotation angle is fixed and an entire island is moved within $\sqrt{3} \times \sqrt{3}$ unit cell until the minimal energy is achieved for a given angle. Then, the procedure is repeated for a set of angles. As a result, one has a dependence of island energy as a function of a rotation angle. In the present simulations, the range of 0° – 30° is explored with a step of 0.1° . The dependence shows a number of minima at selected angles of which the lowest minimum corresponds to an optimal island orientation. In order to test the validity of the proposed surface potential relief, we consider two sample islands: the 37-C₆₀ island (which according to the experiment has to have 0° -rotated orientation and a regular hexagon shape with a bright C₆₀ at its center) and the relatively large 365-C₆₀ island (which according to the experiment has to have 19.1° -rotated orientation and no moiré pattern). One can see that with the given interpolated potential relief the goal is not reached either for small or large islands. In contrast to the experiment, the 10.9° -rotated orientation appears to be the lowest-energy one for both types of islands [Fig. 3(a)].

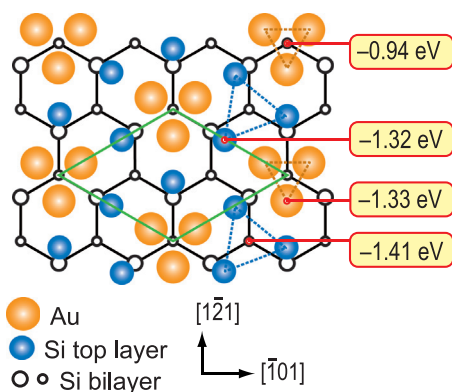


FIG. 2. (Color online) Schematic diagram of Si(111) $\sqrt{3} \times \sqrt{3}$ -Au surface (CHCT model) where C₆₀ adsorption sites are indicated with corresponding calculated adsorption energies taken from Ref. 39. Legend for Au and Si atoms is given in the Figure. Si and Au trimers are outlined by triangles. In atoms (not shown) are hopping between centers of Si trimers.

Modest smearing of the original relief (that is thought to simulate roughly the thermal effects) partially improves the situation: The simulated 37-C₆₀ island adopts the proper 0° -rotated orientation, but the simulated 365-C₆₀ island demonstrates incorrect 30° -rotated orientation [Fig. 3(b)]. Only when the potential relief is further simplified and becomes approximated by just the cosine-shaped peaks, the proper island orientations are obtained: 0° and 19.1° rotation for the 37-C₆₀ and 365-C₆₀ islands, respectively [Fig. 3(c)]. One can also notice a certain resemblance in the internal contrast of the simulated islands and their counterparts in the experimental STM images [Fig. 3(d)]. However, we would like to note that actually the brightness of fullerenes in the STM images and in the simulated islands has a different origin. STM contrast is associated with the topography and/or electron density of states. In the simulated islands, the brighter C₆₀s have a higher energy (i.e., occupy the sites at the potential relief with a higher energy).

With the obtained potential relief, it becomes possible to simulate other islands and assess their energetics. The results of such an evaluation are summarized in Fig. 4 showing normalized energy of C₆₀ islands of various types as a function of island size. The types of islands under consideration are as follows: 0° - and 19.1° -rotated hypothetical islands with a shape of regular hexagons (indicated by open red and blue open hexagons, respectively), 0° -rotated experimentally observed islands, including those with a shape of overlapping hexagons and those of unusual noncompact shapes of stadium, boomerang, and zigzag (indicated by filled red circles), 19.1° -rotated experimentally observed islands having a shape of irregular hexagons (indicated by filled blue circles). One can see that among small islands the “stadium” (13 C₆₀), “boomerang” (19 C₆₀), and “zigzag” (30 C₆₀) are the most energetically favorable islands in agreement with the experiment. They are followed by the 37-C₆₀ 0° -rotated island with a regular hexagon shape. Remarkably, this is the only island of this type (0° -rotated regular hexagons) which has a preference over the similar-size islands of other types. For larger sizes (e.g., 61 C₆₀, 101 C₆₀, etc.), the 0° -rotated regular hexagons become energetically unfavorable. In contrast, 19.1° -rotated regular hexagons are unfavorable at small

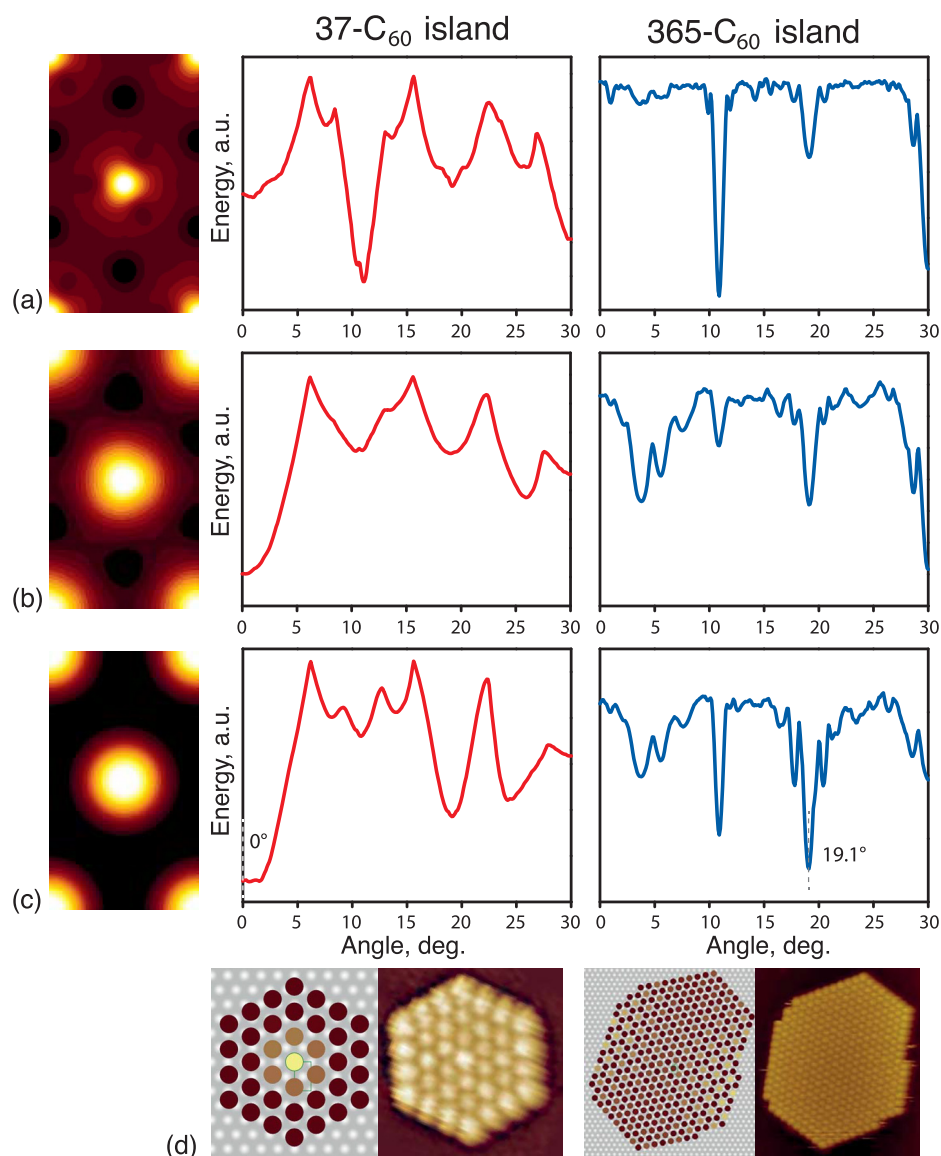


FIG. 3. (Color online) Results of simulations for various shapes of surface potential: (a) interpolated potential, (b) smeared interpolated potential, and (c) cosine-shaped potential for 37-C₆₀ island (left column) and 365-C₆₀ island (right column) presented as the dependencies of normalized island energy vs rotation angle. (d) Experimental STM images of the 0°-rotated 37-C₆₀ and 19.1°-rotated 365-C₆₀ islands vs their simulated counterparts.

sizes but become favorable at sizes above ~ 70 C₆₀ where their energy is comparable with the energy of the 19.1°-rotated irregular hexagons observed in the STM experiments. Note that these islands can be treated as certain derivatives of the hypothetical regular islands. The 0°-rotated islands with a shape of overlapping hexagons have a similar energy to that of large 0°-rotated islands, which justifies the coexistence of islands of both types in the experiment. Thus, simulation reproduces well all the main results of the STM observations on C₆₀ island growth on an In-adsorbed Si(111) $\sqrt{3} \times \sqrt{3}$ -Au surface.

As shown above, the lowest minimum in the dependence of island energy on its rotation angle yields the most preferable orientation of the C₆₀ array. The occurrence of the other minima with a lower depth in such dependence might provide a hint for finding the arrays in alternative less preferable orientations. However, this is not realized in the considered

case of C₆₀ arrays on In-adsorbed Si(111) $\sqrt{3} \times \sqrt{3}$ -Au surface. One possible reason is the relatively strong binding of C₆₀ to this surface, and hence high kinetic barriers. In contrast, the binding of C₆₀ to the Si(111) $\sqrt{3} \times \sqrt{3}$ -Ag surface is less strong and the above consideration can be applied to this system. Moreover, the cosine-type potential relief has been proved to fit this case too rather than potential relief based on DFT calculations.⁵¹ Figure 5 shows the results of simulations of island energy versus rotation angle for the large island containing 271 C₆₀ fullerenes compared to the C₆₀ orientational arrays observed in the experiment. One can see that the lowest minimum in simulations is at the 19.1°-rotation angle in agreement with STM observations showing that the majority of C₆₀ arrays on Si(111) $\sqrt{3} \times \sqrt{3}$ -Ag are in the 19.1°-rotated orientation. However, close examination of STM images enables us to find minor arrays in the orientations predicted by simulations. Broad minima at $\sim 4^\circ$ and

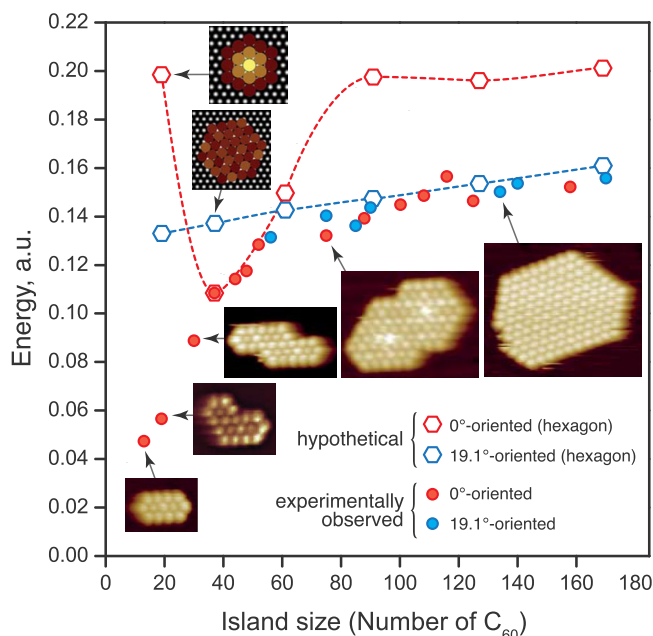


FIG. 4. (Color online) Normalized energy (i.e., energy per C₆₀) of C₆₀ islands of various types as a function of island size (i.e., number of C₆₀ molecules constituting a given island). The types of islands include 0°- and 19.1°-rotated hypothetical islands having a shape of regular hexagons, 0°-rotated experimentally observed islands having a shape of overlapping hexagons as well as unusual shapes of stadium, boomerang, and zigzag, 19.1°-rotated experimentally observed islands having a shape of irregular hexagons. The legend for the corresponding symbols is given in the bottom of the Figure. Dashed lines for hypothetical hexagonal islands are drawn to guide an eye. Representative STM images are shown to illustrate the typical island shapes observed in experiment while simulated images show hypothetical hexagonal islands.

6° do have counterparts in STM images though it is impossible to elucidate accurate correspondence due to the limited accuracy of angle evaluation with STM. The arrays in 10.9°- and 30°-rotated orientations predicted by simulations are also present in reality. One could also expect arrays with rotation angles of ~18° and ~21° due to the occurrence of

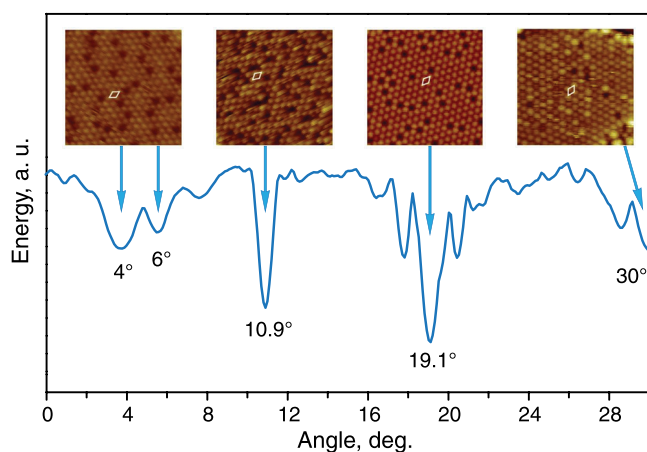


FIG. 5. (Color online) Dependence of island energy vs rotation angle for the simulated large 271-C₆₀ island on Si(111) $\sqrt{3} \times \sqrt{3}$ -Ag surface with indication of correspondence of the minima of the dependence to the orientations of the extended arrays observed in the STM experiment. C₆₀ array unit cells are outlined in the STM images.

corresponding minima, but in the real STM experiments they can hardly be distinguished from the 19.1°-rotated arrays.

Certain differences do exist in the behavior of C₆₀ on In-adsorbed Si(111) $\sqrt{3} \times \sqrt{3}$ -Au and pristine Si(111) $\sqrt{3} \times \sqrt{3}$ -Ag surfaces [e.g., in contrast to the C₆₀/Si(111) $\sqrt{3} \times \sqrt{3}$ -(Au, In) system, no regular moiré pattern develops in C₆₀ layers on an Si(111) $\sqrt{3} \times \sqrt{3}$ -Ag surface, instead there are random dim C₆₀ fullerenes whose appearance was suggested to result from the breaking of the Ag trimers beneath them].⁴³ However, many prominent features for both systems are effectively reproduced by simulations with a qualitatively similar potential relief with cosine-shaped peaks. It is worth noting that the usage of seemingly more accurate potentials that were determined using DFT calculations and that reveal a fine structure of potential relief^{39,43,51} produced poor simulation results. Three possible reasons for the advantage of the simplified potential can be proposed. First, the size of the C₆₀ molecule exceeds the scale of the potential fine structure; thus, fullerene “feels” only the most essential features of the potential relief. Second, while in calculations of a potential as well as in simulations zero temperature is assumed, the real growth of C₆₀ arrays proceeds at a finite temperature and thermal effects (vibration and rotation of the fullerenes) might be visualized as an effective smearing of the potential relief. Third, intermolecular C₆₀-C₆₀ forces may stabilize or destabilize certain positions on the surface, which is not taken into account in the DFT calculations for a single C₆₀ adsorption.

IV. CONCLUSION

In conclusion, the proposed procedure for simulation of self-assembled C₆₀ islands on metal-adsorbed Si(111) surfaces has been proved to be a suitable tool for assessing island energetics, shape, and orientation. Simulation consists of placing a patch of close-packed C₆₀ array of a given shape on a surface potential relief and finding energy minima by variation of island position and orientation. Upon appropriate adjustment of the surface potential relief, simulations reproduce all the main results of STM observations. For C₆₀ islands forming on In-adsorbed Si(111) $\sqrt{3} \times \sqrt{3}$ -Au and pristine Si(111) $\sqrt{3} \times \sqrt{3}$ -Ag surfaces, the optimal surface relief is one that shows up as a periodic array of cosine-shaped peaks. As the present simulations do not rely on any particular feature of the C₆₀ molecule or given reconstruction, in principle, they can be applied to many other adsorbate-substrate pairs.

ACKNOWLEDGMENT

The work was supported by Russian Science Foundation under Grant No. 14-12-00482.

¹H. W. Kroto, J. R. Heath, S. C. O'Brien, R. F. Curl, and R. E. Smalley, *Nature* **318**, 162 (1985).

²X. Lu, M. Grobis, K. H. Khoo, S. G. Louie, and M. F. Crommie, *Phys. Rev. B* **70**, 115418 (2004).

³X. Zhang *et al.*, *Phys. Rev. B* **75**, 235444 (2007).

⁴M. Feng and H. Petek, *Science* **320**, 359 (2008).

- ⁵J. A. Larsson, S. D. Elliott, J. C. Greer, J. Repp, G. Meyer, and R. Allenspach, *Phys. Rev. B* **77**, 115434 (2008).
- ⁶W. W. Pai *et al.*, *Phys. Rev. Lett.* **104**, 036103 (2010).
- ⁷L. Tang, X. Zhang, Q. Guo, Y.-N. Wu, L.-L. Wang, and H.-P. Cheng, *Phys. Rev. B* **82**, 125414 (2010).
- ⁸S. I. Bozhko, S. A. Krasnikov, O. Lübben, B. E. Murphy, K. Radican, V. N. Semenov, H. C. Wu, B. Bulfin, and I. V. Shvets, *Phys. Rev. B* **84**, 195412 (2011).
- ⁹M. Švec, P. Merino, Y. J. Dappe, C. González, E. Abad, P. Jelínek, and J. A. Martín-Gago, *Phys. Rev. B* **86**, 121407 (2012).
- ¹⁰K. Pussi *et al.*, *Phys. Rev. B* **86**, 205406 (2012).
- ¹¹F. Loske, J. Lübbe, J. Schütte, M. Reichling, and A. Kühnle, *Phys. Rev. B* **82**, 155428 (2010).
- ¹²A. V. Matetskiy, L. V. Bondarenko, D. V. Gruznev, A. V. Zotov, A. A. Saranin, J. P. Chou, C. R. Hsing, C. M. Wei, and Y. L. Wang, *Surf. Sci.* **616**, 44 (2013).
- ¹³N. V. Sibirev, V. G. Dubrovskii, A. V. Matetskiy, L. V. Bondarenko, D. V. Gruznev, A. V. Zotov, and A. A. Saranin, *Appl. Surf. Sci.* **307**, 46 (2014).
- ¹⁴M. A. Groce, B. R. Conrad, W. G. Cullen, A. Pimpinelli, E. D. Williams, and T. L. Einstein, *Surf. Sci.* **606**, 53 (2012).
- ¹⁵M. Hinterstein, X. Torrelles, R. Felici, J. Rius, M. Huang, S. Fabris, H. Fuess, and M. Pedio, *Phys. Rev. B* **77**, 153412 (2008).
- ¹⁶X. Torrelles, V. Langlais, M. D. Santis, H. Tolentino, and Y. Gauthier, *J. Phys. Chem. C* **114**, 15645 (2010).
- ¹⁷X. Torrelles, V. Langlais, M. D. Santis, H. C. N. Tolentino, and Y. Gauthier, *Phys. Rev. B* **81**, 041404 (2010).
- ¹⁸X. Torrelles, M. Pedio, C. Cepek, and R. Felici, *Phys. Rev. B* **86**, 075461 (2012).
- ¹⁹H. I. Li *et al.*, *Phys. Rev. Lett.* **103**, 056101 (2009).
- ²⁰X. Q. Shi, A. B. Pang, K. L. Man, R. Q. Zhang, C. Minot, M. S. Altman, and M. A. Van Hove, *Phys. Rev. B* **84**, 235406 (2011).
- ²¹G. Xu, X.-Q. Shi, R. Q. Zhang, W. W. Pai, H. T. Jeng, and M. A. Van Hove, *Phys. Rev. B* **86**, 075419 (2012).
- ²²T. Ovramenko, F. Spillebout, F. C. Bocquet, A. J. Maynei, G. Dujardin, P. Sonnet, L. Stauffer, Y. Ksari, and J.-M. Themlin, *Phys. Rev. B* **87**, 155421 (2013).
- ²³H. Shin *et al.*, *Phys. Rev. B* **89**, 245428 (2014).
- ²⁴A. Tamai, A. P. Seitsonen, F. Baumberger, M. Hengsberger, Z.-X. Shen, T. Greber, and J. Osterwalder, *Phys. Rev. B* **77**, 075134 (2008).
- ²⁵J. D. Sau, J. B. Neaton, H. J. Choi, S. G. Louie, and M. L. Cohen, *Phys. Rev. Lett.* **101**, 026804 (2008).
- ²⁶X. Q. Shi, M. A. Van Hove, and R. Q. Zhang, *Phys. Rev. B* **85**, 075421 (2012).
- ²⁷I. Hamada and M. Tsukada, *Phys. Rev. B* **83**, 245437 (2011).
- ²⁸D. Li, C. Barreteau, A. L. Kawahara, J. Lagoute, C. Chancon, Y. Girard, S. Rousset, V. Repain, and A. Smogunov, *Phys. Rev. B* **93**, 085425 (2016).
- ²⁹N. Martsinovich and L. Kantorovich, *Phys. Rev. B* **77**, 115429 (2008).
- ³⁰N. Martsinovich and L. Kantorovich, *Nanotechnology* **19**, 235702 (2008).
- ³¹N. Martsinovich and L. Kantorovich, *Nanotechnology* **20**, 135706 (2009).
- ³²J. A. Venable, G. D. T. Spiller, and M. Hanbücken, *Rep. Prog. Phys.* **47**, 399 (1984).
- ³³R. Cantrell and P. Clancy, *J. Chem. Theory Comput.* **8**, 1048 (2012).
- ³⁴B. Koo and P. Clancy, *Mol. Simul.* **40**, 58 (2014).
- ³⁵B. Koo, P. Berard, and P. Clancy, *J. Chem. Theory Comput.* **11**, 1172 (2015).
- ³⁶Y. Acevedo, R. Cantrell, P. Berard, D. Koch, and P. Clancy, *Langmuir* **32**, 3045 (2016).
- ³⁷H. Liu, Z. Lin, L. V. Zhigilei, and P. Reinke, *J. Phys. Chem. C* **112**, 4687 (2008).
- ³⁸See supplementary material at <http://dx.doi.org/10.1116/1.4961906> with detailed description of the simulation algorithm.
- ³⁹D. V. Gruznev *et al.*, *Nat. Commun.* **4**, 1679 (2013).
- ⁴⁰A. V. Matetskiy, D. V. Gruznev, A. V. Zotov, and A. A. Saranin, *Phys. Rev. B* **83**, 195421 (2011).
- ⁴¹T. Nakayama, J. Onoe, K. Takeuchi, and M. Aono, *Phys. Rev. B* **59**, 12627 (1999).
- ⁴²K. Tsuchie, T. Nagao, and S. Hasegawa, *Phys. Rev. B* **60**, 11131 (1999).
- ⁴³D. V. Gruznev, A. V. Matetskiy, L. V. Bondarenko, A. V. Zotov, A. A. Saranin, J. P. Chou, C. M. Wei, and Y. L. Wang, *Surf. Sci.* **612**, 31 (2013).
- ⁴⁴Y. G. Ding, C. T. Chan, and K. M. Ho, *Surf. Sci.* **275**, L691 (1992).
- ⁴⁵I. H. Hong, D. K. Liao, Y. C. Chou, C. M. Wei, and S. Y. Tong, *Phys. Rev. B* **54**, 4762 (1996).
- ⁴⁶J. Y. Lee and M. H. Kang, *J. Korean Phys. Soc.* **55**, 2460 (2009).
- ⁴⁷T. Nagao, S. Hasegawa, K. Tsuchie, S. Ino, C. Voges, G. Klos, H. Pfnür, and M. Henzler, *Phys. Rev. B* **57**, 10100 (1998).
- ⁴⁸D. V. Gruznev, I. N. Filippov, D. A. Olyanich, D. N. Chubenko, I. A. Kuyanov, A. A. Saranin, A. V. Zotov, and V. G. Lifshits, *Phys. Rev. B* **73**, 115335 (2006).
- ⁴⁹J. K. Kim, K. S. Kim, J. L. McChesney, E. Rotenberg, H. N. Hwang, C. C. Hwang, and H. W. Yeom, *Phys. Rev. B* **80**, 075312 (2009).
- ⁵⁰L. V. Bondarenko *et al.*, *Sci. Rep.* **3**, 1826 (2013).
- ⁵¹S. Jeong, *J. Phys. Soc. Jpn.* **79**, 074603 (2010).